Optical Materials 121 (2021) 111630

Contents lists available at ScienceDirect

Optical Materials

journal homepage: www.elsevier.com/locate/optmat

Research Article

Defect assisted optical limiting performance of hexagonal boron nitride nanosheets in aqueous suspension and PMMA nanocomposite films

Bekir Asilcan Unlu [a], Ahmet Karatay [a,*], Elif Akhuseyin Yildiz [a], Mehmet Lutfi Yola [b], Mustafa Yuksek [c], Necip Atar [d], Ayhan Elmali [a]

[a] Department of Engineering Physics, Faculty of Engineering, Ankara University, 06100, Beşevler, Ankara, Turkey
[b] Hasan Kalyoncu University, Faculty of Health Sciences, Department of Nutrition and Dietetics, Gaziantep, Turkey
[c] Iskenderun Tech Univ, Fac Engn & Nat Sci, Dept Elect Elect Engn, TR-31200, Iskenderun, Hatay, Turkey
[d] Pamukkale University, Faculty of Engineering, Department of Chemical Engineering, Denizli, Turkey

ARTICLE INFO

Keywords:
Boron nitride
Nanosheet
Optical limiting
Nonlinear absorption
Photoluminescence

ABSTRACT

Defect-assisted nonlinear absorption (NLA) and optical limiting (OL) performance of hexagonal boron nitride nanosheets (h-BNNS) in aqueous suspension and in polymethyl methacrylate matrix (PMMA) as nanocomposite films were studied using open-aperture Z-scan method. To evaluate the transmission in open-aperture *Z*-scan data, a theoretical model accounting one photon absorption (OPA), two photon absorption (TPA), free carrier absorption (FCA) and saturation of each process was considered. Defect-assisted NLA coefficients and saturation intensity thresholds were extracted from the fitting of the experimental results for 532 and 1064 nm pulse wavelengths. Strong defect-assisted NLA response of h-BNNS was observed while NLA at 532 nm was considerably stronger. This is attributed to the excitation of a greater number of defect states over a wider energy range. Our findings showed that h-BNNS/PMMA nanocomposite films feature highly required properties in OL applications and can function in OL applications in a wide spectral range (~200–1064 nm).

1. Introduction

Two-dimensional (2D) hexagonal boron nitride (h-BN) is an important member of the 2D material family since 2D h-BNNS (known as white graphene in literature) provide good temperature stability, mechanical strength, thermal conductivity and large surface area [1–3]. Defect-free h-BNNS with boron and nitrogen (N) atoms strongly bonded in a 2D honeycomb lattice is chemically and thermally stable. These properties allow h-BNNS to be widely used as sensors, catalysts, bioimaging and drug delivery systems. In particular, the transparency feature in visible and IR regions indicates the large band gap (~6 eV) of h-BNNS. The wide band gap energy allows for a wider range of band engineering compared to the zero-band gap graphene [4–7].

h-BN contains an abundance of structural defects that can be formed during synthesis or following treatments [8–11]. Understanding and controlling the effects of defects on electronic and optical properties in h-BN is crucial for future technological developments. Generally, carrier localization occurring on defect states could reduce the carrier mobility and trapping/de-trapping of carriers at these states could enhance noise levels and limit the exploitation in devices. However, point defects in h-BN layers can create energy levels within the bandgap and modify local electronic structures to provide magnetic and photonic functionalities [12,13]. Point defects are also significant for quantum technologies, where they serve as recombination centers for quantum emissions and can be adapted to behave as ultra-bright emitters with narrow linewidth [14]. h-BN possess various types of defects such as point defects as vacancies, substitutional and interstitial, line defects as dislocations and planar defects as grain boundaries [15]. All these defect types tailor the electronic structure in addition to modifying the local atomic structure [16].

Although studies on defect engineering of h-BN samples are in their infancy, results have been obtained indicating that optical features of h-BN can be manipulated by introducing or altering point defects. Optical features can be adjusted potently by vacancy construction and external electric fields [17–19]. Vacancy construction yields an exciton emission by introducing localized defect states within the band gap, whereas an external electric field lead to the manipulation of vacancies such as the migration or diffusion of the vacancies yielding the construction of new

* Corresponding author.
E-mail address: akaratay@eng.ankara.edu.tr (A. Karatay).

https://doi.org/10.1016/j.optmat.2021.111630
Received 3 August 2021; Received in revised form 16 September 2021; Accepted 26 September 2021
Available online 1 October 2021

emission behaviors. Hence, the effects of defects on the properties of h-BN and engineering of these defects possess an immense amount of importance nowadays. However, there are limited studies on NLA properties of h-BN, to the best of our knowledge only Xie et al., Dong et al. and Kumbhakar et al. reported the NLA of h-BN in aqueous dispersions and moreover, the effect of defects on NLA was not considered [20–22]. The main aim of this work is to investigate the defect assisted NLA properties with a model accounting OPA, TPA and FCA of h-BNNS samples especially in solid thin film form which is sought for optical applications. The photoluminescence (PL) results of h-BNNS reporting emissions at way lower energies than its band gap energy due to defect states residing deep inside band gap and the wide band gap energy of h-BNNS due to its insulator nature reveals the possibility of a NLA behavior and OL performance at high light intensity regions [23–25]. In OL applications there is an urgent need for materials showing limiting behavior in a wide wavelength range, as most OL materials function in a limited region in the visible region or even in infrared and near infrared region of the spectrum. A secondary focus of this study is to examine OL performance due to the defect assisted NLA.

2. Experimental methods

Following the preparation of bulk BN (100.0 mg) dispersion in isopropyl alcohol (50.0 mL), the heating treatment was performed at 50 °C for 24 h under stirring. Then, the dispersion was subjected to ultrasonication for 15 h. After the centrifugation at 20000 rpm for 5 min, the precipitate was washed with acetone several times and dried at 50 °C overnight to obtain 2D h-BNNS. To coat h-BNNS on fused silica substrates, 150 g/L solution of PMMA in cyclohexanone was placed in sonic bath for 72 h until PMMA is completely dissolved. h-BNNS was then added to the solution and left on a magnetic stirrer for 4 h until a homogeneous dispersion was obtained. Solid thin films of the samples were coated on quartz substrates by using spin coating method (SCS-Spin Coat G3P). Obtained films were baked at 100 °C for 2 h to remove the residual solvent and kept in vacuum for 24 h. Nanocomposite films were prepared at two different concentrations in PMMA matrix, with 10 and 15 wt%.

Following the coating of h-BNNS/PMMA nanocomposite films, the thickness measurements were carried out using spectroscopic ellipsometer (M2000V (J.A. Woollam Co.). The film thicknesses were determined as 1.5 μm at three incidence angles of 60°, 65°, 70° in the photon energy range between 1.26 eV and 3.10 eV. UV–Vis absorption spectrophotometer (Shimadzu UV-1800) was used to record the absorption spectra of the films. PL measurements were recorded using a Fluorescence Spectrometer (PerkinElmer LS55). SEM images and EDX pattern of h-BNNS samples were obtained by ZEISS EVO 40 (500 V–30 kV) scanning electron microscope. TEM images of h-BNNS samples were obtained by FEI Tecnai G2 (200 kV) transmission electron microscope. Open aperture (OA) Z-scan method was performed to investigate the NLA properties of the samples using Q-switched Nd:YAG laser (Quantel Brillant) with 532 nm and 1064 nm wavelength, 4 ns pulse duration and 10 Hz repetition rate.

3. Results and discussions

3.1. Material characterization

Scanning electron microscope (SEM) and transmission electron microscope (TEM) images of h-BNNSs are shown in Fig. 1(a) and (b). Boron nitride particles are stacked vertically due to the weak van der Waals interactions between two-dimensional honeycomb structures composed of strongly bound boron and nitrogen atoms as seen from Fig. 1(a) [26]. SEM image also revealed that boron and nitride atoms form particles with a maximum diameter size of 200 nm (Fig. 1(a), inset image). TEM image taken following the ultrasonication process of h-BNNS in ethanol shows that particles are dispersed but still tend to aggregate in small clusters (Fig. 1(b)). Careful investigation through TEM images also revealed that particles are in diameter size between 50 nm and 200 nm. The B and N atoms in h-BNNS can be substituted during the sample preparation or subsequent treatment. Krivanek et al. have utilized an atom-by-atom analysis and identified three types of atomic substitutions: C substituting for B, C substituting for N, and O substituting for N [27]. The result of EDX analysis (Fig. 1(c)) revealed that in addition to the B and N atoms in h-BNNS, O and C impurity atoms are also present in the h-BNNS structure.

Bulk h-BN has been calculated to possess a band gap between 2.9 and 4.9 eV with varying stacking structures, which is reduced by 0.2–1.5 eV compared to single-layer h-BN [28]. Multilayer and bulk h-BN are wide-bandgap semiconductors that exhibit insignificant linear absorption in the visible spectrum (390 ~ 700 nm). For this reason, they appear white in color and are often called as “white graphene” [29,30]. However, pure h-BNNSs display a substantial amount of absorption in the ultraviolet (UV) region between 200 and 220 nm [31]. A sharp luminescence peak and a few free exciton absorption bands have been

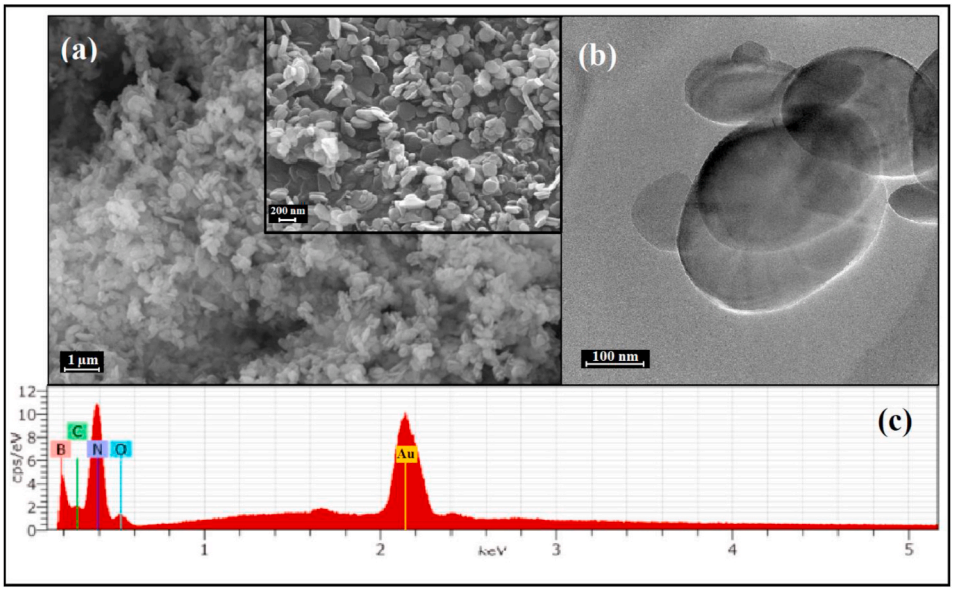

Fig. 1. (a) SEM images, (b) TEM image and (c) the EDX pattern of h-BNNS.

observed at approximately 220 nm for pure h-BN single crystals [32]. Pure h-BNNSs also display an evident cathodoluminescence emission in the deep UV region [33,34]. However, pure h-BNNS only emits in UV region and possess poor optical activity due to the large band gap and absence of defect states [35]. Recently, defect engineering has been developed in order to regulate band gaps of h-BNNSs for the enhancement of photocatalytic activity. Point defects are excessively desirable in UV and visible light luminescence, as they function as recombination centers [36,37]. These point defects provide a way of designing highly efficient quantum fluorescent materials, making h-BNNS applicable in nanophononics and optoelectronics fields.

Fig. 2(a) shows the linear absorption spectra of h-BNNSs dispersed in de-ionized water with different concentrations. Initially a dispersion at a concentration of 150 μg/mL kept in a cuvette of 1 mm path length with 90% linear optical transmittance was obtained to minimize the linear absorption and study the NLA mechanisms where NLA mechanisms are dominant. However, an absorption edge could not be observed in the spectra owing to the insulator nature of h-BNNS sample with large band gap energy. It is considered that the sharp increase in absorption might be occurring at wavelengths less than 190 nm and this is verified by increasing the suspension concentrations until the absorption edge red shifts into the spectra due to the aggregation of nanosheets. A similar result also obtained for h-BNNS/PMMA nanocomposite films where absorption edge of h-BNNS could not be observed. Fig. 2(b) presents the linear absorption spectra of h-BNNS nanocomposite films and pure PMMA. An increase in overall absorption and due to defect states a slowly increasing trend of absorption towards absorption edge can be seen. Even though there might be an increase in absorbance with h-BNNS concentration in PMMA matrix, the slope of the absorption edge and the region where the absorption edge is occurred remain constant, suggesting that the observed absorption edge belongs to the PMMA and overshadows the absorption edge of h-BNNS. In order to estimate the band gap energy of h-BNNSs, photoluminescence (PL) measurements were performed.

Fig. 3 inset shows the emission spectra of the h-BNNS dispersion under 6.20 eV excitation energy. A structured broadband between 300 and 450 nm is observed and in literature it is attributed to the radiative recombination of deep donor-acceptor pairs resulting from defects of boron-nitrogen vacancies and carbon-oxygen impurities occupying the vacancies [23,38,39]. While it is not possible to obtain an estimation of band gap energy from PL emission spectra because radiative recombination occurs via defect levels and yields emission energies much lower than band gap energy, excitation spectra can be used to estimate band gap energy by obtaining excitation wavelength where the maxima of PL emission band (350 nm) demonstrates a sharp increase. The excitation spectra of the h-BNNS dispersion is depicted in Fig. 3. According to the figure the emission at 350 nm wavelength starts at excitation wavelength of 220 nm (~5.65 eV) and reaches its peak value at 207 nm (~6.00 eV). The strong emission peaking at excitation energy of 6.00 eV is in good agreement with the band gap results in the literature [24,34,39].

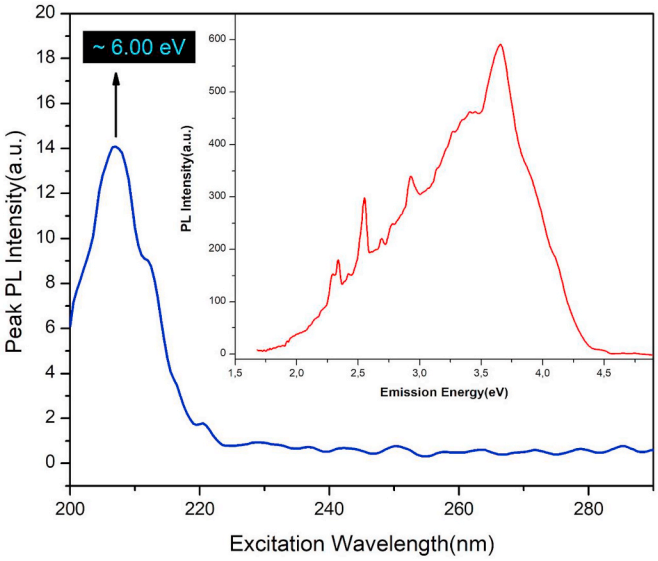

Fig. 3. PL excitation spectra of h-BNNS suspension and (inset) PL emission spectra of h-BNNS suspension.

3.2. Defect assisted nonlinear absorption and optical limiting performance

Various defects, such as vacancies, grain boundaries, interstitial and substitution atoms can be observed in h-BNNSs due to the synthesis process or subsequent treatments [40–42]. Moreover, dopant atoms, e.g., hydrogen [43], carbon [27], oxygen [44], and fluorine [45] are

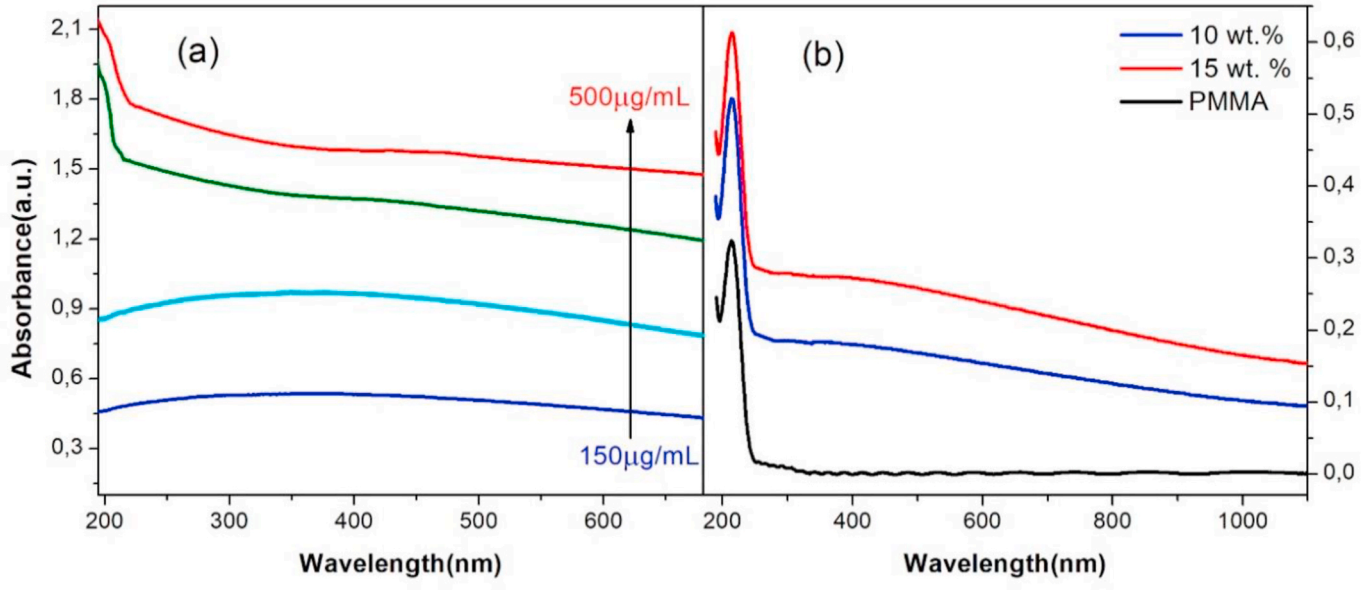

Fig. 2. Linear absorption spectra of (a) suspension and (b) h-BNNS/PMMA nanocomposite films.

typical types of defects in h-BNNS. These defects create an opportunity to open up new possibilities of tuning the electronic and optical properties of h-BNNS by altering the type and concentration of defects.

It is particularly expected that an abundance of structural defects observed in h-BNNS seriously shapes the NLA behavior through defect states. Therefore, to study defect assisted NLA, a model that considers OPA, TPA, FCA and saturation of each absorption mechanisms were considered [46–48].

$$\frac{dI}{dz} = -\frac{\alpha I}{1 + I/I_{sat}} - \frac{\beta I^2}{1 + I^2/I_{sat}^2} - \frac{\sigma_o \Delta N(I) I}{1 + I^2/I_{sat}^2} \quad (1)$$

In Eq. (1) first, second and third term accounts for OPA, TPA and FCA, respectively. σ_o is FCA cross section, α is OPA coefficient and β is TPA coefficient. $\Delta N(I)$ is photoexcited free carrier density and depends on the intensity. I_{sat} is saturation intensity threshold.

Photoexcited free carrier density can be written in terms of α and β as [49].

$$\Delta N = \frac{\alpha I}{\hbar\omega}\tau_0 + \frac{\beta I^2}{2\hbar\omega}\tau_0 \quad (2)$$

Where τ_0 is pulse duration, $\hbar\omega$ is photon energy. By substituting photo excited free carrier density equation into Eq. (1) the following equation can be obtained.

$$\frac{dI}{dz} = -\frac{\alpha I}{1 + I/I_{sat}} - \frac{\beta_{eff} I^2}{1 + I^2/I_{sat}^2} \quad (3)$$

β_{eff} term in above equation is effective NLA coefficient and includes the contribution of both FCA and TPA. TPA has the weakest contribution to free carrier generation, therefore it was neglected in the FCA term in Eq. (3) and β_{eff} was expressed as $\beta_{eff} = \beta + (\sigma_o \alpha \tau_0 / \hbar\omega)$.

The Adomian decomposition method was used to solve Eq. (3) and fit the experimental OA Z-scan curves. A detailed information about the model can be found in the literature [47,48].

The experimental data obtained by OA Z-scan measurements and the theoretical fits derived from Eq. (3) covering β_{eff} and I_{sat} as free parameters are given in Fig. 4(a) and (b). β_{eff} and I_{sat} values that are obtained from theoretical fits are given in Table 1.

In a sample with non-overlapping energy bands and defect levels residing within band gap, TPA can occur in two ways. Interband TPA can occur when the energy of a single photon is less than the band gap energy but greater than half the band gap energy and the probability of TPA increases as the photon energy approaches the band gap energy. Sub-band gap TPA can occur when the combined energy of two photons is sufficient to induce an electron transition between energy bands and defect states.

Table 1
The β_{eff} and I_{sat} values obtained from the OA Z-scan experiments with 1064 nm wavelength and 532 nm.

Samples	1064 nm Results		532 nm Results	
	β_{eff} (cm/GW)	I_{sat} (GW/cm^2)	β_{eff} (cm/GW)	I_{sat} (GW/cm^2)
Suspension	4.86×10^2	2.39	5.62×10^2	4.12
Film (10 wt%)	6.42×10^5	5.03	7.05×10^5	7.97
Film (15 wt%)	1.05×10^6	8.08	1.52×10^6	8.18

In 1064 nm experiments, the transitions occur through TPA since PL emission occurring in the range of 2.0–4.2 eV with a peak at 3.66 eV corresponds to defect states residing deep inside band gap [38]. Energy corresponding to 1064 nm wavelength (1.16 eV) is not sufficient to induce OPA. In 532 nm wavelength experiments TPA occurs stronger and is accompanied by OPA, since the photon energy of 2.32 eV corresponds to a wider energy region in the band gap and sufficient to induce electron transitions between energy bands and defect states. In addition, time-and energy-resolved PL experiments have shown that there is a slow recombination component (22–200 ns) for h-BNNS corresponding to the broadband in PL emission (Fig. 3 inset) [23]. Slow recombination time inferring to long defect state lifetimes also suggest that TPA occurs via the sequential absorption of two photons rather than simultaneous absorption of two photons since the pulse duration of 4 ns is shorter than the lifetime of defect states. Simultaneous TPA occurs via a virtual state and thus requires rather high excitation intensities, on the other hand sequential TPA occurring through intermediate defect states (real states) dominates in low excitation intensity regimes. Hence activation of OPA with 532 nm also leads to sequential TPA in addition to simultaneous TPA and overall NLA performance gets enhanced by the increased energy range of 532 nm laser wavelength compared to that of 1064 nm. In 532 nm experiments, a stronger TPA accompanied also by OPA reveals an increased NLA behavior for h-BNNS which is seen as a further decreased transmittance (see Fig. 4(b) compared to Fig. 4(a)) and as increased β_{eff} values when comparing the result at 532 nm and 1064 nm in Table 1. When the results at 532 nm and 1064 nm are evaluated

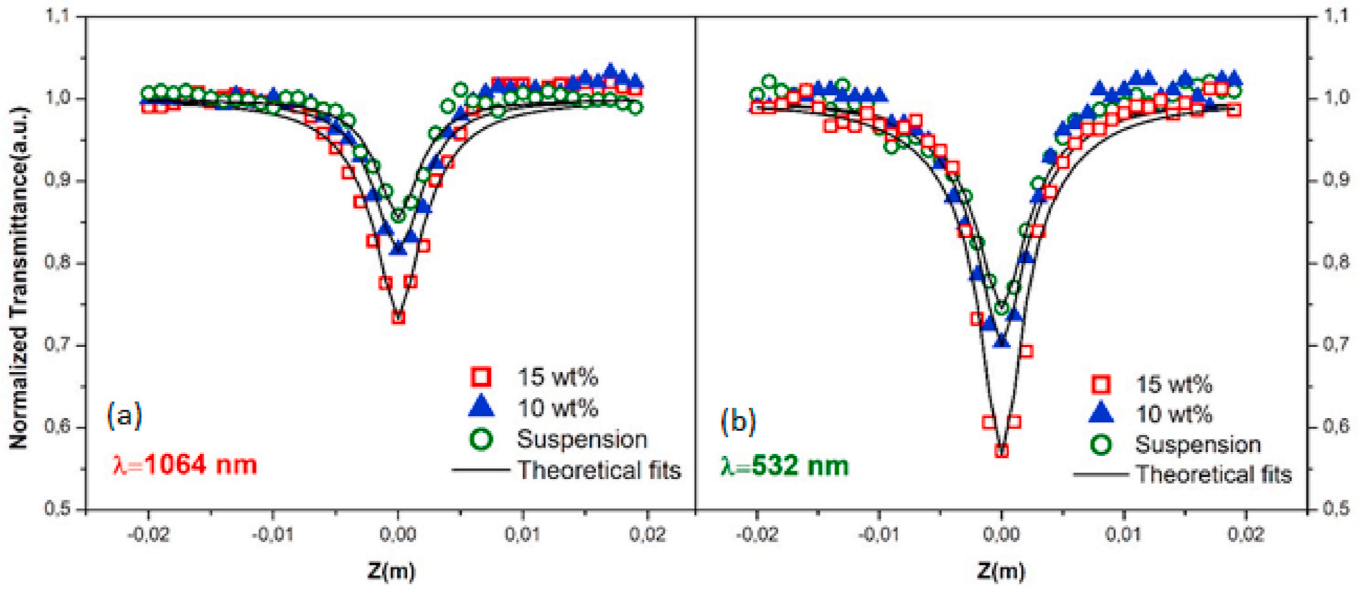

Fig. 4. Open aperture Z-scan traces of h-BNNS samples at (a) 1064 nm and (b) 532 nm wavelengths (I = 62.1 MW/cm^2).

separately for each wavelength it is observed that between 10 wt% and suspension samples, 10 wt% film yields a higher β_{eff} since the concentration of h-BNNS is significantly higher in h-BNNS/PMMA nanocomposite films than that of in suspension and 15 wt% film exhibits the highest NLA performance. I_{sat} values also display the same tendency to increase as the h-BNNS concentration, with increased h-BNNS content in the samples defect states also increase and the saturation of the defect states becomes increasingly difficult. 15 wt% film possesses the highest I_{sat} value and suspension possesses the smallest I_{sat} value. On the other hand, Kumbhakar et al. have conducted nonlinear optical experiments on h-BNNSs in aqueous dispersions and attributed the strong NLA behavior of h-BNNSs to strong polar behavior of the electronegativity difference between B and N atoms [22], herein we put forth the dominant source of NLA of h-BNNS as defect states that reside within band gap. Conducting OA Z-scan experiments at a single light intensity to induce the same nonlinear polarization response but with two different wavelengths revealed that by decreasing the wavelength of laser, NLA can be enhanced and since the experiments with smaller wavelength cover a wider energy range, more defect states can be excited.

Despite its insulating nature, h-BNNS's strong NLA behavior over a wide spectrum of wavelengths prompted us to examine the OL performance of h-BNNS samples. One of the most important features searched in OL materials is having low optical transparency in high intensity regimes while having high optical transparency in low intensity regimes. In other words, the material with low linear absorption and high NLA properties is expected to display limiting behavior. Since h-BNNS is an insulator with a wide band gap, it satisfies the low linear absorption condition (see Fig. 2(b)), and OA Z-scan experiments prove that h-BNNS displays significant NLA behavior over a wide spectrum. Therefore, the fluence dependent optical transmission data of 15 wt% nanocomposite film which has the best NLA response and suspension which has the worst NLA response, were calculated from the OA Z-scan curves, and featured in Fig. 5. The normalized transmittance remains constant at low input fluence and at higher fluence values the horizontal transmittance curve start to fall, that is, NLA begins to occur and material begins to limit the transmitted light. The fluence value at which the normalized transmittance starts to decrease, in other words OL threshold values are found to be 0.98 mJ/cm^2 and 2.20 mJ/cm^2 for nanocomposite film at 532 nm and 1064 nm wavelengths and it is found to be 3.88 mJ/cm^2 and 8.57 mJ/cm^2 for suspension at 532 nm and 1064 nm wavelengths. Due to the increased h-BNNS concentration in nanocomposite film form, OL performance in solid film form is found to be superior to the suspension form, and the fact that the defect levels are spread over within the band gap (as seen from the broadband emission in Fig. 3 inset) indicates that the film samples can be used for OL not only in the 532–1064 nm wavelength range also in the 200–1064 nm wavelength range as well.

4. Conclusions

We have investigated the defect assisted NLA and OL of h-BNNSs in aqueous suspension and nanocomposite films. Linear absorption and PL measurements revealed that h-BNNS had ~6 eV band gap and large number of defect states reside deep inside band gap. To investigate the defect assisted NLA we considered a theoretical model incorporating OPA, TPA, FCA and their saturations. Due to the defect states within the band gap, all of the h-BNNS samples showed significant NLA response when interacting with intense laser light with under both 532 and 1064 wavelengths while the NLA at 532 nm were considerably stronger. Samples showing defect assisted NLA behavior over a wide wavelength range despite being insulators with a wide band gap, revealed that especially h-BNNS/PMMA nanocomposite film samples can be used in OL applications in a wide wavelength range (~200–1064 nm) due to their high linear transmittance and low OL threshold. Our findings showed that defect density tunability opens up the possibility of using h-BNNS in tunable optical device applications. h-BNNS has an abundant amount of defect states. Achieving a defect density tunability with h-BNNS also reveals that other 2D materials with fewer defect states can be exploited by defect density tuning more precisely to the point of either nonlinear absorption or saturable absorption is achieved. Changing the behavior of the material between a nonlinear absorber and a saturable absorber offers the possibility to use 2D wide band gap materials even at opposite ends of the application fields, such as optical limiting where a strong nonlinear absorber is required, and q-switching where a saturable absorber is.

CRediT authorship contribution statement

Bekir Asilcan Unlu: Investigation, Research, Data curation, Visualization, Writing – review & editing. **Ahmet Karatay:** Supervision, Conceptualization, Methodology, Writing – review & editing. **Elif Akhuseyin Yildiz:** Investigation, Writing – review & editing. **Mehmet Lutfi Yola:** Conceptualization, Methodology, Resources. **Mustafa Yuksek:** Conceptualization, Methodology. **Necip Atar:** Conceptualization, Methodology, Resources. **Ayhan Elmali:** Project administration,

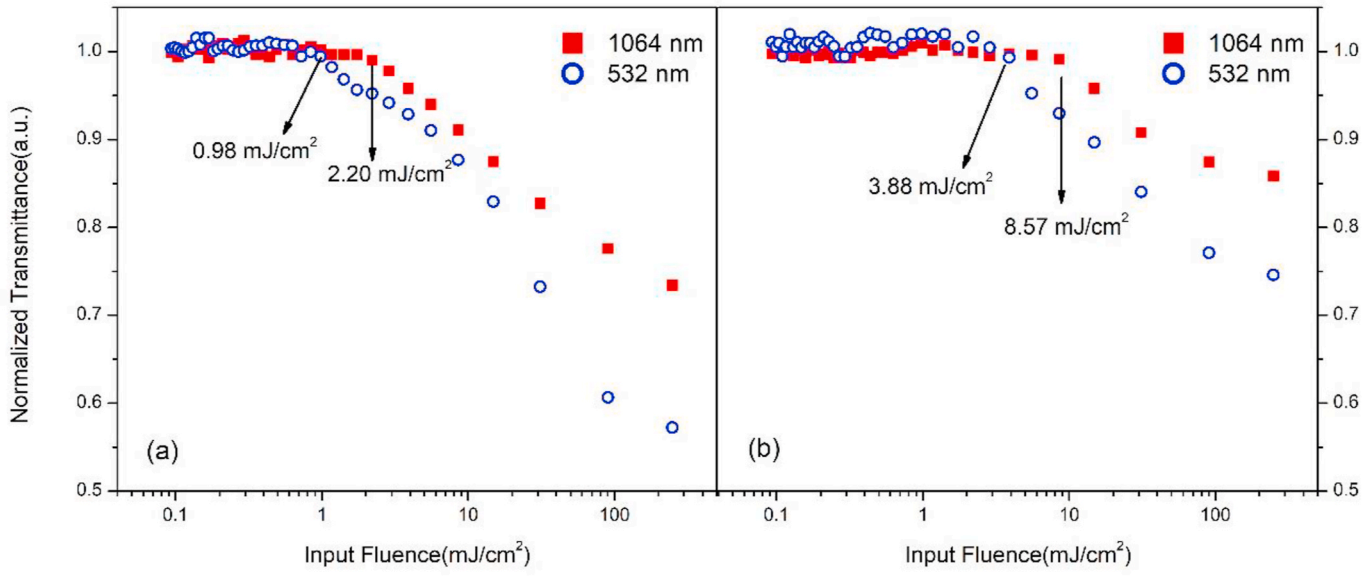

Fig. 5. Fluence dependent nonlinear optical transmittance of (a) 15 wt% h-BNNS/PMMA thin film and (b) h-BNNS suspension.

Conceptualization, Methodology, Writing – review & editing.

Declaration of competing interest

The authors declare that they have no known competing financial interests or personal relationships that could have appeared to influence the work reported in this paper.

References

[1] G.Y. Lu, T.R. Wu, Q.H. Yuan, H.S. Wang, H.M. Wang, F. Ding, X.M. Xie, M.H. Jiang, Nat. Commun. 6 (2015).
[2] F.N. Xia, H. Wang, D. Xiao, M. Dubey, A. Ramasubramaniam, Nat. Photonics 8 (2014) 899–907.
[3] L. Wang, X.Z. Xu, L.N. Zhang, R.X. Qiao, M.H. Wu, Z.C. Wang, S. Zhang, J. Liang, Z. H. Zhang, Z.B. Zhang, W. Chen, X.D. Xie, J.Y. Zong, Y.W. Shan, Y. Guo, M. Willinger, H. Wu, Q.Y. Li, W.L. Wang, P. Gao, S.W. Wu, Y. Zhang, Y. Jiang, D. P. Yu, E.G. Wang, X.D. Bai, Z.J. Wang, F. Ding, K.H. Liu, Nature 570 (2019) 91–+.
[4] A.L. Gibb, N. Alem, J.H. Chen, K.J. Erickson, J. Ciston, A. Gautam, M. Linck, A. Zettl, J. Am. Chem. Soc. 135 (2013) 6758–6761.
[5] N.R. Jungwirth, B. Calderon, Y.X. Ji, M.G. Spencer, M.E. Flatte, G.D. Fuchs, Nano Lett. 16 (2016) 6052–6057.
[6] N. Alem, O.V. Yazyev, C. Kisielowski, P. Denes, U. Dahmen, P. Hartel, M. Haider, M. Bischoff, B. Jiang, S.G. Louie, A. Zettl, Phys. Rev. Lett. 106 (2011).
[7] C.H. Jin, F. Lin, K. Suenaga, S. Iijima, Phys. Rev. Lett. 102 (2009).
[8] S. Susarla, P. Manimunda, Y.M. Jaques, J.A. Hachtel, J.C. Idrobo, S.A.S. Asif, D. S. Galvao, C.S. Tiwary, P.M. Ajayan, Adv Mater Interfaces 6 (2019).
[9] J.H. Warner, E.R. Margine, M. Mukai, A.W. Robertson, F. Giustino, A.I. Kirkland, Science 337 (2012) 209–212.
[10] C.O. Girit, J.C. Meyer, R. Erni, M.D. Rossell, C. Kisielowski, L. Yang, C.H. Park, M. F. Crommie, M.L. Cohen, S.G. Louie, A. Zettl, Science 323 (2009) 1705–1708.
[11] K. Jasuja, K. Ayinde, C.L. Wilson, S.K. Behura, M.A. Ikenbbery, D. Moore, K. Hohn, V. Berry, ACS Nano 12 (2018) 9931–9939.
[12] R. Bourrellier, S. Meuret, A. Tararan, O. Stephan, M. Kociak, L.H.G. Tizei, A. Zobelli, Nano Lett. 16 (2016) 4317–4321.
[13] Q.H. Weng, G.D. Li, X.L. Feng, K. Nielsch, D. Golberg, O.G. Schmidt, Adv. Mater. 30 (2018).
[14] T.T. Tran, K. Bray, M.J. Ford, M. Toth, I. Aharonovich, Nat. Nanotechnol. 11 (2016) 37–+.
[15] N. Alem, Q.M. Ramasse, C.R. Seabourne, O.V. Yazyev, K. Erickson, M.C. Sarahan, C. Kisielowski, A.J. Scott, S.G. Louie, A. Zettl, Phys. Rev. Lett. 109 (2012).
[16] H. Li, C. Tsai, A.L. Koh, L.L. Cai, A.W. Contryman, A.H. Fragapane, J.H. Zhao, H. S. Han, H.C. Manoharan, F. Abild-Pedersen, J.K. Norskov, X.L. Zheng, Nat. Mater. 15 (2016).
[17] T. Jia, Z. Zeng, X.L. Zhang, P. Ohodnicki, B. Chorpening, G. Hackett, J. Lekse, Y. H. Duan, Phys. Chem. Chem. Phys. 21 (2019) 20454–20462.
[18] L.P. Feng, J. Su, Z.T. Liu, J. Alloys Compd. 613 (2014) 122–127.
[19] P. Modak, B. Modak, Phys. Chem. Chem. Phys. 22 (2020) 16244–16257.
[20] Z. Xie, Y.Z. Wu, X.M. Sun, S.X. Liu, F.K. Ma, G. Zhao, X.P. Hao, S.Y. Zhou, Nanoscale 10 (2018) 4276–4283.
[21] Y.C. Dong, P. Parajuli, A.M. Rao, W. Thielemans, S. Eyley, K.R. Sahoo, T. N. Narayanan, R. Podila, Opt. Mater. 86 (2018) 414–420.
[22] P. Kumbhakar, A.K. Kole, C.S. Tiwary, S. Biswas, S. Vinod, J. Taha-Tijerina, U. Chatterjee, P.M. Ajayan, Adv Opt Mater 3 (2015) 828–835.
[23] L. Museur, E. Feldbach, A. Kanaev, Phys. Rev. B 78 (2008).
[24] S. Biswas, C.S. Tiwary, S. Vinod, A.K. Kole, U. Chatterjee, P. Kumbhakar, P. M. Ajayan, J. Phys. Chem. C 121 (2017) 8060–8069.
[25] M.S. Jin, N.O. Kim, J Electr Eng Technol 5 (2010) 637–639.
[26] T.Q.P. Vuong, S. Liu, A. Van der Lee, R. Cusco, L. Artus, T. Michel, P. Valvin, J. H. Edgar, G. Cassabois, B. Gil, Nat. Mater. 17 (2018) 152–+.
[27] O.L. Krivanek, M.F. Chisholm, V. Nicolosi, T.J. Pennycook, G.J. Corbin, N. Dellby, M.F. Murfitt, C.S. Own, Z.S. Szilagyi, M.P. Oxley, S.T. Pantelides, S.J. Pennycook, Nature 464 (2010) 571–574.
[28] H. Sahin, S. Cahangirov, M. Topsakal, E. Bekaroglu, E. Akturk, R.T. Senger, S. Ciraci, Phys. Rev. B 80 (2009).
[29] J.N. Coleman, M. Lotya, A. O'Neill, S.D. Bergin, P.J. King, U. Khan, K. Young, A. Gaucher, S. De, R.J. Smith, I.V. Shvets, S.K. Arora, G. Stanton, H.Y. Kim, K. Lee, G.T. Kim, G.S. Duesberg, T. Hallam, J.J. Boland, J.J. Wang, J.F. Donegan, J. C. Grunlan, G. Moriarty, A. Shmeliov, R.J. Nicholls, J.M. Perkins, E.M. Grieveson, K. Theuwissen, D.W. McComb, P.D. Nellist, V. Nicolosi, Science 331 (2011) 568–571.
[30] M.S. Long, P. Wang, H.H. Fang, W.D. Hu, Adv. Funct. Mater. (2019) 29.
[31] K.K. Kim, A. Hsu, X.T. Jia, S.M. Kim, Y.S. Shi, M. Hofmann, D. Nezich, J. F. Rodriguez-Nieva, M. Dresselhaus, T. Palacios, J. Kong, Nano Lett. 12 (2012) 161–166.
[32] K. Watanabe, T. Taniguchi, H. Kanda, Nat. Mater. 3 (2004) 404–409.
[33] A. Nag, K. Raidongia, K.P.S.S. Hembram, R. Datta, U.V. Waghmare, C.N.R. Rao, ACS Nano 4 (2010) 1539–1544.
[34] Y. Kubota, K. Watanabe, O. Tsuda, T. Taniguchi, Science 317 (2007) 932–934.
[35] A. Pakdel, Y. Bando, D. Golberg, Chem. Soc. Rev. 43 (2014) 934–959.
[36] S.A. Tawfik, S. Ali, M. Fronzi, M. Kianinia, T.T. Tran, C. Stampfl, I. Aharonovich, M. Toth, M.J. Ford, Nanoscale 9 (2017) 13575–13582.
[37] C. Palacios-Berraquero, D.M. Kara, A.R.P. Montblanch, M. Barbone, P. Latawiec, D. Yoon, A.K. Ott, M. Loncar, A.C. Ferrari, M. Atature, Nat. Commun. 8 (2017).
[38] B. Berzina, V. Korsaks, L. Trinkler, A. Sarakovskis, J. Grube, S. Bellucci, Diam. Relat. Mater. 68 (2016) 131–137.
[39] Q.X. Wang, Q. Zhang, X.X. Zhao, X. Luo, C.P.Y. Wong, J.Y. Wang, D.Y. Wan, T. Venkatesan, S.J. Pennycook, K.P. Loh, G. Eda, A.T.S. Wee, Nano Lett. 18 (2018) 6898–6905.
[40] Y.F. Zhukovskii, S. Bellucci, S. Piskunov, L. Trinkler, B. Berzina, Eur Phys J B 67 (2009) 519–525.
[41] A.S. Vokhmintsev, I.A. Weinstein, M.G. Minin, S.A. Shalyakin, Radiat. Meas. 124 (2019) 35–39.
[42] Y. Liu, Z.B. Tan, M. Kumar, T.S. Abhilash, G.J. Liu, P. Hakonen, Apl. Mater. 6 (2018).
[43] X.X. Li, J. Zhao, J.L. Yang, Sci Rep-Uk 3 (2013).
[44] G.Y. Gou, B.C. Pan, L. Shi, J. Am. Chem. Soc. 131 (2009) 4839–4845.
[45] C. Chen, J.M. Wang, D. Liu, C. Yang, Y.C. Liu, R.S. Ruoff, W.W. Lei, Nat. Commun. 9 (2018).
[46] A. Karatay, C. Aksoy, H.G. Yaglioglu, A. Elmali, U. Kurum, A. Ates, N. Gasanly, J Optics-Uk 13 (2011).
[47] M. Yuksek, U. Kurum, H.G. Yaglioglu, A. Elmali, A. Ates, J. Appl. Phys. 107 (2010).
[48] U. Kurum, M. Yuksek, H.G. Yaglioglu, A. Elmali, A. Ates, M. Karabulut, G. M. Mamedov, J. Appl. Phys. 108 (2010).
[49] N. Kamaraju, S. Kumar, A.K. Sood, S. Guha, S. Krishnamurthy, C.N.R. Rao, Appl. Phys. Lett. 91 (2007).